Utah State University

DigitalCommons@USU

5-6-2021

Phase-Space Dynamics of Runaway Electrons in Tokamaks

Gavin Held
Utah State University

Follow this and additional works at: https://digitalcommons.usu.edu/phys_capstoneproject

Part of the Physics Commons

Recommended Citation

UtahStateUniversity
MERRILL-CAZIER LIBRARY

Phase-Space Dynamics of Runaway Electrons in Tokamaks⋆

Gavin W. Held*, and Eric D. Held

Department of Physics, Utah State University, Logan, UT 84322-4415, USA

Abstract

Nuclear fusion converts the rest mass energy of ions like the deuteron and triton into kinetic energy. In theory, this energy can be harvested from a thermonuclear reactor to provide power outputs on the scale of 500 MW. High temperatures are needed for significant fusion to occur, hence the tokamak (a modern fusion confinement device) employs strong magnetic fields to keep the ionized gas (plasma) away from the tokamak wall. However, a problem that occasionally arises in a tokamak is that during a disruption an inductive electric field is created which can accelerate electrons to relativistic speeds (these electrons are called runaway electrons (RE's)). The magnetic field lines also become stochastic (volume-filling) and can intersect with the wall. Following magnetic field lines, RE's are led to and can obliterate the expensive plasma facing components (PFC's). This work involves getting the physics of RE's into NIMROD, a plasma-fluid code. Overall, this is a very large and complex problem so we will focus on seeing if NIMROD's relativistic electron model agrees with other 2D phase-space codes in terms of how the electrons get accelerated. This involves looking at the different processes: acceleration by the inductive electric field, the drag force associated with colliding off the background plasma, and the release of energy through synchrotron radiation. Considering all of this we want to see if NIMROD can predict/calculate a balance of these forces to lead to a steady state vortex pattern in the relativistic phase-space.

Keywords: Magnetically confined plasmas, drift-kinetic theory, runaway electrons
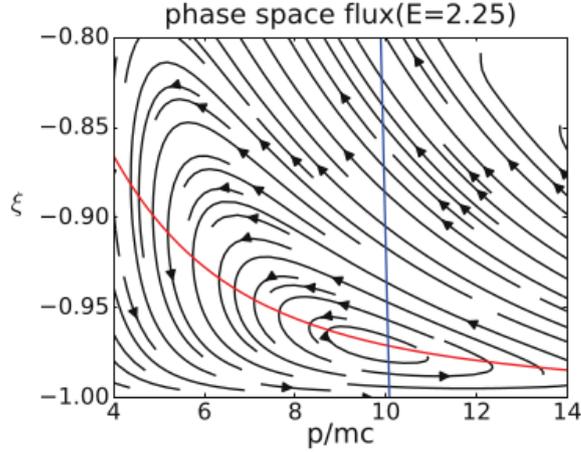
Figure 1: Plot of the steady-state flow pattern in a 2D relativistic phase space consisting of normalized relativisitc momentum, $p/m_e c$, along the x-axis and cosine of pitch angle, $p_\parallel/p$, along the y–axis, where $p_\parallel$ is the particle's momentum along the magnetic field. This depicts the "O" point from Guo, the center of the vortex pattern in phase space flux where both the energy flux Γ_p (represented by the red line) and pitch-angle flux Γ_ξ (represented by the blue line) are zero.

1. Introduction

Tokamak disruptions are characterized by a rapid loss of plasma thermal energy and current. When a tokamak disrupts, an electric field is induced. Electrons can *runaway* to speeds close to the speed of light if this inductive electric field is greater than what is called the critical field $E_c = n_e e^3 ln\Lambda/(4\pi\epsilon_0^2 m_e c^2)$ [1, 2]. Here n_e, e, and m_e are the number density, charge, and rest mass of the electron, ϵ_o is the permittivity of free space, and $ln\Lambda$ is the Coulomb Logarithm, typically on the order of 20 for the weakly coupled plasmas of modern tokamaks. Physically, this critical field arises from a balance of the accelerating force of the electric field and the drag force due to binary collisions of the relativistic electrons with the background, thermal plasma. This runaway behavior occurs because as an electron's velocity increases, the collisional friction with the background plasma decreases. The part of the electron distribution with $p > m_e c$ is able to overcome the collisional damping and continuously accelerates to relativistic speeds.

A ton of research effort and money has been put into the runaway electron (RE) problem in tokamaks. A nice review article on REs is given in Ref. [2]. Most of the work in this document is related to Refs. [1] and [3]. Information on the form of the Coulomb collision operator for ultra-relativistic electrons is given in Ref. [4] and an appendix of Ref. [5] discusses its generalization to map onto non-relativistic distributions. In this work we use the numerical methods described in Ref. [6] to advance a relativistic population of electrons in the presence of a background thermal plasma. The goal is to benchmark NIMROD's RE implementation against previous results, specifically the vortex dynamics presented in Ref. [3] and shown in Figs.1 and 2. The steady-state flow pattern in the 2D relativistic phase space results from a balance between the accelerating electric field (chosen to be parallel to the magnetic field) and the dissipative effects of radiation damping and collisions in cases where E is close to E_c. In the full-blown simulations presented at the end of this document, $E/E_c = 2.25$ as in the Guo reference[3]. The distribution function for steady-state vortex pattern is also shown in Fig. 2 on the right. Our goal is to reproduce the distribution function in Fig. 2 by doing the same problem but using the NIMROD code [7].

Before proceeding to the full, phase-space vortex problem, we first discuss a simpler test of the numerical algorithm in NIMROD, namely, the free acceleration of an isotropic, relativistic Maxwell-Jüttner distribution. This will allow us to discuss some of the basics of relativistic plasma kinetics as well as benchmark the code on a simple problem.
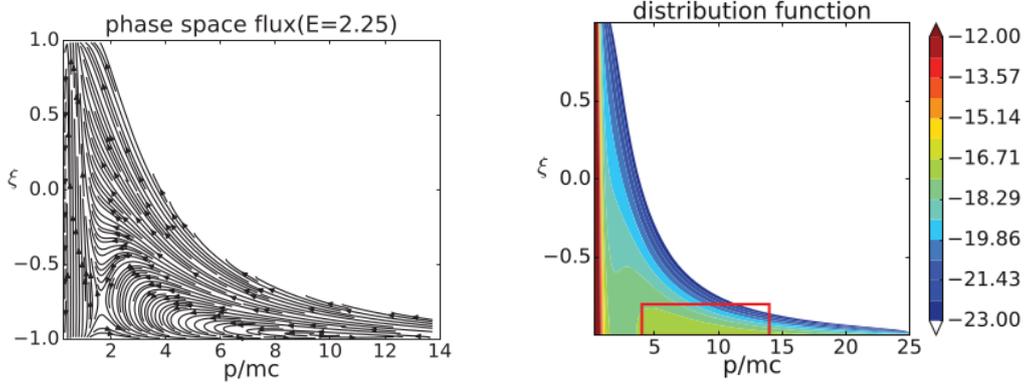
Figure 2: The plot on the left is again of the steady-state flow pattern in a 2D relativistic phase space consisting of normalized relativisitc momentum and cosine of pitch angle, but is instead zoomed out to show the whole vortex pattern. The plot on the right shows the distribution function for the vortex pattern with respect to the normalized momentum $p/m_e c$ and cosine of pitch angle $p_\parallel/p$.

2. Non-relativistic and Relativistic Distribution Functions

When dealing with distributions of nonrelativistic particles, one makes use of the equilibrium, Maxwell–Boltzmann distribution, which has the form

$$f_{MB}(v) = \frac{n}{\pi^{3/2} v_T^3} e^{-v^2/v_T^2}. \tag{1}$$

Here v is the speed, n is the number density, and the thermal speed $v_T = \sqrt{2kT/m}$, where m is the rest mass, k is Boltzmann's constant, and T is the temperature. One can use this distribution to calculate different moments which describe the macroscopic behavior of the population of particles.

In this research, however, we are specifically considering REs, which travel near the speed of light, so the non-relativisitic Maxwell-Boltzman distribution does not suffice. A distribution that takes into account special relativity is needed. In relativistic kinetic theory, the correct equilibrium distribution is given by the Maxwell-Jüttner form, namely,

$$f_{MJ}(p) = \frac{n}{4\pi c^3 \Theta K_2(1/\Theta)} e^{-\sqrt{1+p^2}/\Theta}, \tag{2}$$

where n is the number density in the lab frame and the relativistic expression for normalized momentum $p = \gamma m v/mc$ with $\gamma = 1/\sqrt{1 - v^2/c^2} = \sqrt{1 + p^2}$. Here v and c are the particle speed and speed of light, respectively, $K_2(1/\Theta)$ is a modified Bessel functions of the 2nd kind (a.k.a. the MacDonald function), and $\Theta = kT/(mc^2)$. One can similarly calculate moments that describe its macroscopic behavior. One of the relevant moments in this research is the relativistic momentum density moment which is defined as

$$\mathbf{P} = \frac{1}{m^3} \int d^3\mathbf{p} f(p)\mathbf{p}. \tag{3}$$

Here $\mathbf{p}$ on the right has units of momentum and $\mathbf{P}$ on the right has units of momentum density. We will discuss this moment again later in terms of the free acceleration test.

Before moving on, we would like to show that by starting with the Maxwell-Jüttner distribution, one can retrieve the non-relativistic distribution. We assume that $\Theta << 1$, *i.e.* the nonrelativistic limit, and expand the MacDonald function $K_n(1/\Theta)$ as

$$K_n(\frac{1}{\Theta}) \approx \sqrt{\frac{\pi\Theta}{2}} e^{-1/\Theta} \left[1 + (\frac{4n^2 - 1}{8(1/\Theta)}(1 + \frac{(4n^2 - 3^2)}{2(8(1/\Theta))}(...) \right] \approx \sqrt{\frac{\pi\Theta}{2}} e^{-1/\Theta}. \tag{4}$$

3

Substituting this approximation into the Maxwell-Jüttner distribution leads to the kinetic energy appearing in the exponent. With some maniputlation, it eventually yields

$$f_{MJ} \simeq \frac{\sqrt{2}}{4} \frac{n}{c^3} \left(\frac{mc^2}{\pi kT}\right)^{3/2} e^{-(\gamma mc^2 - mc^2)/kT} \simeq \frac{n}{\pi^{3/2} v_T^3} e^{-v^2/v_T^2}, \tag{5}$$

which is the Maxwellian-Boltzmann distribution in Eq. 1.

3. Free Acceleration Test

If a constant electric field is applied, the Maxwell-Jüttner distribution in Eq. 2 simply accelerates with all of the electrons obeying the relativistic form of Newton's 2nd Law,

$$\frac{d\gamma mv}{dt} = -eE. \tag{6}$$

Here we assume that the electron population does not interact with itself. A constant electric field, E, allows for simple integration to yield $mv = -eEt \sqrt{1 - v^2/c^2}$ where we assume that the electron starts from rest. Solving for v/c yields

$$\frac{v(t)}{c} = \frac{-(eEt/mc)}{\sqrt{1 + (eEt/mc)^2}} = \frac{-(E/|E|)}{\sqrt{1 + (1/t^*)^2}}, \tag{7}$$

where t^* in the final expression has been normalized to the acceleration time, $mc/(eE)$.

We can simulate the same effect using the continuum relativistic electron model in NIMROD by advancing

$$\frac{\partial f_e}{\partial t} - \frac{eE}{mc} \left(\xi \frac{\partial f_e}{\partial p} + \frac{(1 - \xi^2)}{p} \frac{\partial f_e}{\partial \xi} \right) = 0. \tag{8}$$

Here the normalized relativistic momentum is still $p = \gamma mv/mc = \gamma v/c$, its normalized directed component along the electric field is $\xi = p_\parallel/p$, and f_e starts out as an isotropic, Maxwell-Jüttner distribution for a collection of relativistic electrons in equilibrium. Discretizing in time using a θ-centered advance yields

$$\Delta f_e - \theta \Delta t \frac{eE}{mc} \left(\xi \frac{\partial \Delta f_e}{\partial p} + \frac{(1 - \xi^2)}{p} \frac{\partial \Delta f_e}{\partial \xi} \right) = \Delta t \frac{eE}{mc} \left(\xi \frac{\partial f_e^k}{\partial p} + \frac{(1 - \xi^2)}{p} \frac{\partial f_e^k}{\partial \xi} \right), \tag{9}$$

where $\Delta f_e = (f_e^{k+1} - f_e^k)$ is the change in the distribution function over the time step Δt. Again measuring time in units of the constant acceleration time, $mc/(eE)$, yields the relatively simple expression

$$\Delta f_e - \theta dt \left(\xi \frac{\partial \Delta f_e}{\partial p} + \frac{(1 - \xi^2)}{p} \frac{\partial \Delta f_e}{\partial \xi} \right) = dt \left(\xi \frac{\partial f_e^k}{\partial p} + \frac{(1 - \xi^2)}{p} \frac{\partial f_e^k}{\partial \xi} \right), \tag{10}$$

where $dt = \Delta t/(mc/(eE))$ and $\theta = 1$ ($\theta = 0$) effects a fully implicit (explicit) advance.

Expanding on what is meant by Δf_e, we define it as

$$\Delta f_e = \sum_{l=0} \Delta f_l(p) P_l(\xi), \tag{11}$$

where $P_l(\xi)$ are chosen to be Legendre polynomials for the free acceleration test and $\Delta f_l(p)$ are the p-dependent coefficients of those polynomials.

We can then muliply each side by $P_{l'}(\xi)$ and integrate over $d\xi$ as follows

$$\int_{-1}^{1} d\xi' P_{l'} \Delta f_e = \sum_{l=0} \Delta f_l(p) \int_{-1}^{1} d\xi P_{l'} P_l.$$

This approach puts the time-derivative along the diagonal of a set of coupled, ordinary differential equations for the vector of p-dependent coefficients based on the orthogonality of Legendre polynomials, namely,

$$\int_{-1}^{1} d\xi' P_{l'} P_l = \frac{2}{2l+1} \delta_{ll'}.$$

Then, the coupled system that NIMROD solves looks like

$(\mathbf{M}_t - \theta\Delta t(\mathbf{M}_p \frac{\partial}{\partial p} + \mathbf{M}_\xi))\Delta\mathbf{f} = \Delta t(\mathbf{M}_p^k \frac{\partial}{\partial p} + \mathbf{M}_\xi^k)\mathbf{f}^k.$

Finally, a collocation approach is used in p to convert the coupled system of ODEs into a linear system of the form $\mathbf{A}\Delta\mathbf{f} = \mathbf{b}$, which is solved using NIMROD's preconditioned GRMES algorithm.

3.0.1. Results of Free Acceleration Test

For this benchmark, we initialize an isotropic Maxwell-Jüttner distribution and let it accelerate freely according to Eq. 9. The initial shape of the distribution function, which is isotropic in $\xi = p_\parallel/p$, is shown on the left side of Figs. 3, 4 and 5. If the numerical method were exact, that shape would be maintained as the entire distribution accelerations freely to the right with the same time dependence as Eq. 7. We can test various levels of numerical resolution to determine how much is needed to preserve the shape of the distribution, and also yield a macropscopic flow moment consistent with Eq. 7.

The results of running NIMROD for a free acceleration are shown in Figs.3-5. To produce the plots for the initial conditions (t=0) we edited how many collocation points (np) were used in each run from 10, to 20 to 40. We advanced each of the setups for a total of 500 time steps, with each time step corresponding to $dt = \Delta t/(mc/eE) = 0.01$. This amounts to five acceleration times. On the right of Figs. 3, 4 and 5 we show the distribution after 100 time steps, or one acceleration time. Looking at Fig.3 we see that unlike all the others it is mostly green, which represents values of zero for that particular plot. This shows that one cannot advance the code for very long before it falls apart if you only use 10 collocation points. However, once you add more collocation points, the shape of the distribution is preserved for longer periods of time. If one wanted to, one could continue doubling the number of points past 40. This assumes you have the computational power and patience to do so.

Another way to check the fidelity of the numerical approach to this problem is to consider moments of f_e. During simulations of relativistic electron kinetics, NIMROD can also calculate different moments of the distribution as functions of time. One important moment (mentioned previously in Eq. 3) is related to the normalized flow moment. We are interested in comparing to the relativistic velocity derived from Newton's 2nd law (Eq. 7), which says that a single electron acted on by a constant electric field will accelerate asymptotically to $v/c = 1$. The fluid moment that should behave identically to the single particle picture is the normalized parallel flow moment,

$$\frac{V_\parallel(t)}{c} = \frac{P_\parallel}{\gamma(V_\parallel/c)nmc} = \frac{2\pi}{m^3\gamma(nmc)} \int_{-1}^{1} d\xi\xi \int_0^\infty dp p^3 f_e,$$

Here f_e is defined as $f_e(p,\xi) = \sum_{l=0} f_l(p)P_l(\xi)$. Given $P_1(\xi) = \xi$, the integral becomes

$$\frac{V_\parallel(t)}{c} = \frac{2\pi}{m^3\gamma(nmc)} \sum_{l=0} \int_0^\infty dp p^3 f_l(p) \int_{-1}^{1} d\xi P_1(\xi)P_l(\xi) = \frac{4\pi}{3\gamma n} \int_0^\infty dp p^3 f_1(p).$$

The results of actually running the code, computing the $V_\parallel/c$ moment and comparing with Newton's 2nd law are shown in Fig. 6. As you can see there are four different curves. The squares shows $v(t^*)/c$, and the three solid lines are the flow moments for different numbers of p collocation points, 10, 20 and 40. The three lines follow Newton's 2nd law for a bit but eventually succumb to errors in the distribution function which lead to an inaccurate momentum density (relativistic flow) moment. As the number of collocation points is increased, the distribution function maintains its shape (see Figs. 3, 4 and 5 on the right) thus resulting in a more accurate flow moment. However, it is interesting to note that the flow moment still asymptotes to c long after the shape of the distribution has been compromised (not shown). This is because the P_1 coefficient can still be relatively accurate, while the coefficents of the higher-order Legendre polynomials needed for maintaining the shape of f_e are not.

We now move on to the full vortex dynamics problem by including the dissipative effects of collisions and synchrotron radiation.
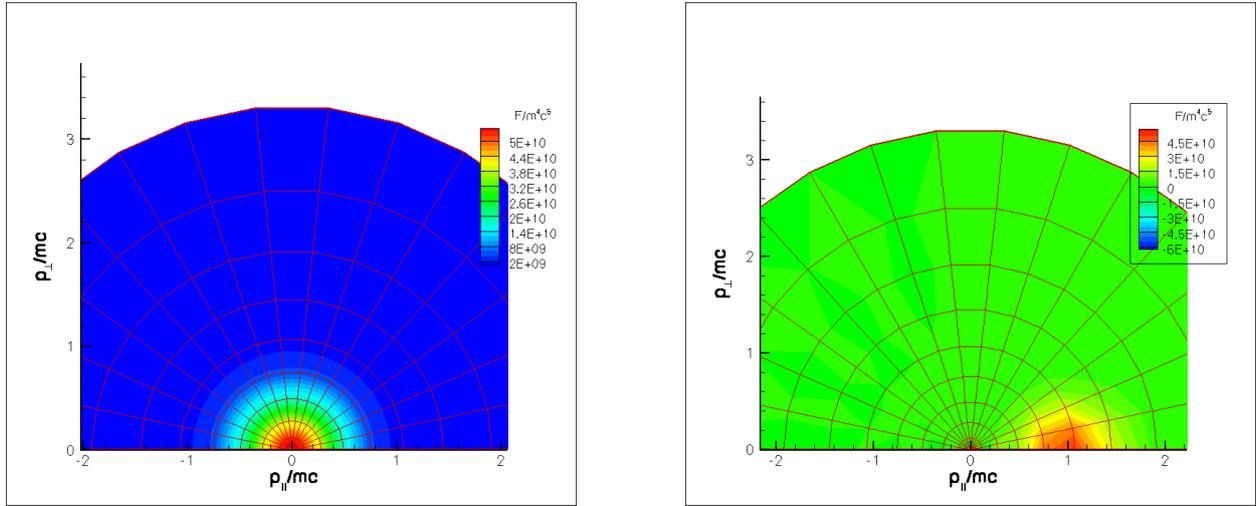
Figure 3: Electron distribution in phase-space with 16 Legendre polynomials (l=0 to 15) for the ξ representation and $np = 10$ collocation points in normalized momentum, p. The the contour on the left is the distribution at t=0 and the one on right is after 100 time steps or one acceleration time ($t^* = 1$), using the same contour levels. The contour on the right should look like the one on the left but simply shifted over. However, the shape has pretty drastically changed.
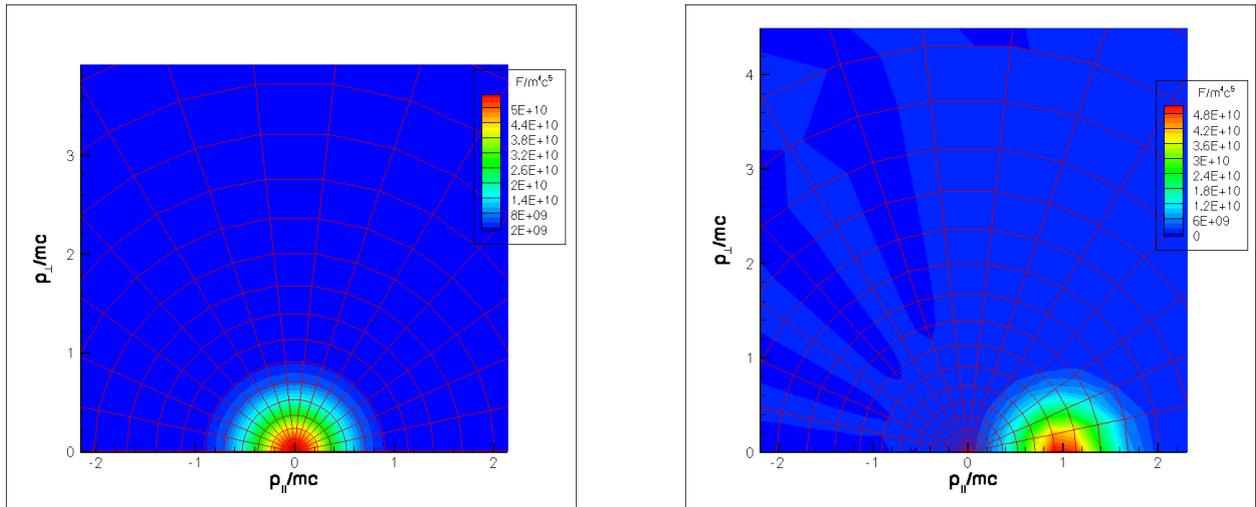

Figure 4: Electron distribution in phase-space with 16 Legendre polynomials (l=0 to 15) for the ξ representation and $np = 20$ collocation points in normalized momentum, p. The the contour on the left is the distribution at t=0 and on the right is after 100 time steps or t^*=1. Here the shape is preserved much better than in the $np = 10$ case.
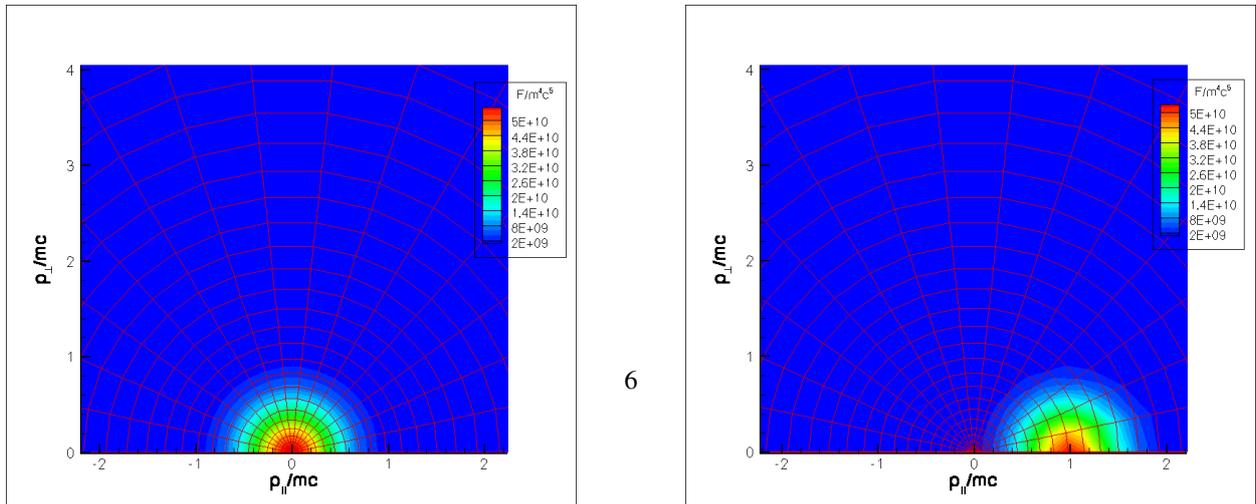

6

Figure 5: Electron distribution in phase-space with 16 Legendre polynomials (l=0 to 15) for the ξ representation and $np = 40$ collocation points in normalized momentum, p. The the contour on the left is the distribution at t=0 and on the right is after 100 time steps or one accleration time. With a more refined p grid, the shape of f_e is well preserved at $t^* = 1$ and for a little while longer.
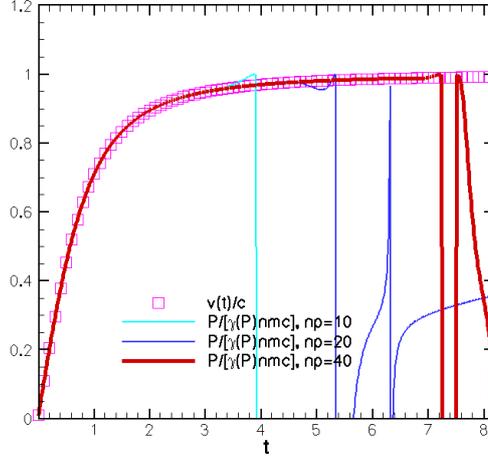
Figure 6: Plot of relativistic flow moments and the solution to Newton's 2nd Law with normalized time (t*) along the x-axis and normalized (wrt. c) velocity along the y-axis. The squares represent the solution of Newton's 2nd Law, namely, $v(t^*)/c = 1/\sqrt{1 + (1/t^*)^2}$, and the curves show how $V_\parallel(t^*)/c$ improves in going from $np = 10$ to $np = 20$ to $np = 40$ with 16 Legendre polynomials.

4. Conservative Form of the Relativistic Kinetic Equation

For the vortex problem, it is prudent to start by discussing the conservative form mentioned in the Guo reference. The conservative form of the relativistic drift kinetic equation with parallel acceleration, collisions, and synchrotron radiation is

$$\frac{\partial f_e}{\partial t} + \frac{1}{p^2}\frac{\partial}{\partial p}\left(p^2\Gamma_p\right) + \frac{1}{p}\frac{\partial}{\partial \xi}\Gamma_\xi = 0. \tag{12}$$

Here the flux in energy (p) is

$$\Gamma_p = -\left[\frac{E}{E_c}\xi + \frac{\tau_c}{\tau_s}p\gamma(1-\xi^2) + C_F + C_A\frac{\partial}{\partial p}\right]f_e$$

and the flux in the pitch-angle-type variable, $\xi = p_\parallel/p$, is

$$\Gamma_\xi = \left[-\frac{E}{E_c}(1-\xi^2) + \frac{\tau_c}{\tau_s}\frac{p}{\gamma}(\xi-\xi^3) - \frac{C_B}{p}(1-\xi^2)\frac{\partial}{\partial \xi}\right]f_e.$$

The time scale of synchrotron radiation damping $\tau_s = 6\pi\epsilon_0 m_e^3 c^3/e^4 B^2$, the time scale for collisions with the background plasma, $\tau_c = 4\pi\epsilon_0 m_e^2 c^3/e^4 n_e ln\Lambda$, and $E_c = m_e c/e\tau_c$ is referred to as the Connor-Hastie field. This is the critical electric field at which relativistic electrons are generated from the tail of a distribution for electrons with normalized momenta $p > 1$. The collisional coefficients, which arise from the effects of binary, small-angle, Coulomb scattering events of a diffuse relativistic population off of thermal, non-relativistic electron and ion distributions, are $C_F = 2(c/v_t)^2\Psi(x)$, $C_A = 2(\gamma/p)\Psi(x)$, and $C_B = 0.5(\gamma/p)[Z + \phi(x) - \Psi(x) + 0.5(v_t/c)^4 x^2]$, where Z is the ion charge (which stems from collisions between relativistic electrons and background ions), $x = (c/v_t)p/\gamma$, $\phi(x)$ is the gamma function, and the Chandrasekhar function $\Psi(x) = (1/2x^2)[\phi(x) - xd\phi/dx]$. Here the collisional coefficients overlap between the non-relativistic and relativistic domains around $p \sim 0.2 - 0.5$. This form for the linearized collision operator arises from the fact that the ultra-relativistic version can be asymptotically matched onto the non-relativistic version. As an example, we show the collision operator coefficients, C_F, C_A and C_B/p^2 for the Guo vortex problem
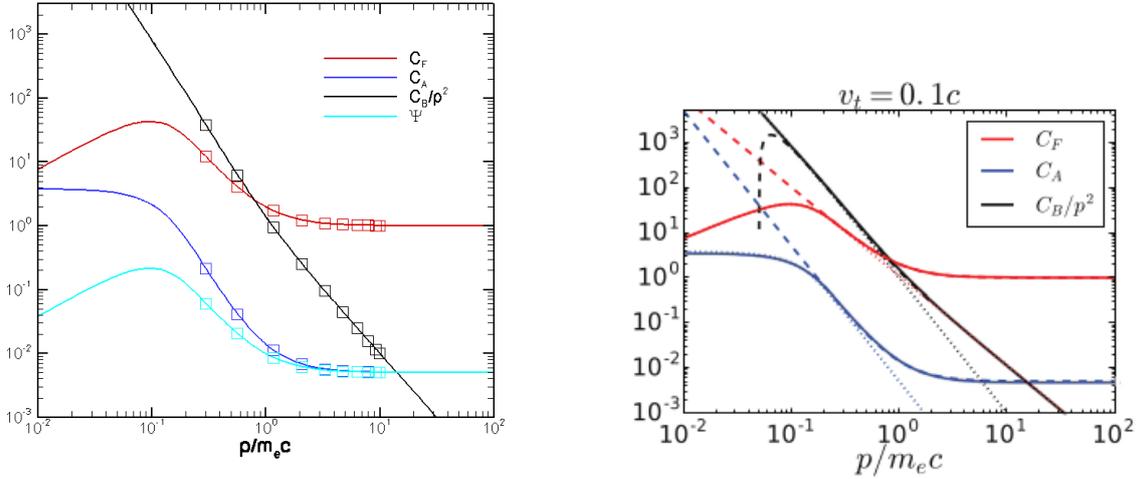
7

Figure 7: Plots of the three collisional coefficients, C_F, C_A, and C_B/p^2 (as well as the Chandresekahr function $\Psi(x)$ on the left) for the parameters of $\Theta_b = 1/200$ meaning the background plasma has $v_T = 0.1c$. On the left we have the results from running the code in NIMROD. On the right we have the results form [3]: the dotted lines correspond to the non-relativistic form, the dashed lines to the relativistic form, and the solid lines are the matched results from their code.

with $v_T = 0.1c$ which corresponds to $\Theta_b = 1/200$ (which is the Θ parameter for the background plasma) on a domain $p \in [0.3, 10]$ with 10 collocations points and fixed points in the p-grid at $p = 0.3$ and $p = 10$. For the relativistic test particle distribution, we have taken $\Theta = 1$. This particular case is discussed last in the following section.

We now proceed to discuss continuum solutions to the full, relativistic electron drift kinetic equation using the implementation in NIMROD.

5. Results for the Phase-Space Vortex Problem

After having implemented the code for the entire relativistic equation into NIMROD, we looked to set up the initial and boundary conditions the same as in the Guo paper.

Rather particular boundary conditions are applied in the vortex dynamics calculation presented by Guo. To prevent energy from leaving the domain, they set $\Gamma_p = 0$ at $p = p_{max}$. This amounts to writing

$$\Gamma(p_{max}) = -\left[\frac{E}{E_c}\xi + \frac{\tau_c}{\tau_s}p_{max}\gamma_{max}(1 - \xi^2) + C_F(p_{max}) + C_A(p_{max})\frac{\partial}{\partial p}|_{p_{max}}\right]f_e = 0.$$

This then specifies the distribution function in terms of its derivative there. When implemented properly, this keeps things settled down on the boundary and should permit evolving to the steady state predicted by Guo. A problem arises, however, namely keeping the distribution function positive everywhere. The advection terms above seems to need some numerical dissipation. This will be the subject of future work. At the lower boundary, the Guo paper assumes that the collisionality is high enough that the distribution function is fixed and the accelerating electric field has no effect. Also synchrotron radiation is assumed to be minimal there. So then, for "computational efficiency" Guo has the distribution function at the lower boundary $p_{min} = v_t$ set to $f_M \sim exp(-2\sqrt{1 + p^2}/v_t^2)$.

Returning back to the collisional coefficients (C_A, C_F, C_B/p^2), the results from running the simulation in NIMROD with the same initial setup as in the Guo paper shows that our coefficients match the Guo results almost identically (both shown in Fig.11). This is quite encouraging as it means we have implemented the collisional the same. Then looking at Fig. 8, we can see how the coefficients change if we adjust the initial conditions (in this case the Θ_b to 1/5). The curves seem to level out for the most part, and this is due to the physics of the background plasma being different (namely it is at a hotter temperature), which alters the collisional damping that the relativistic distribution has with it.
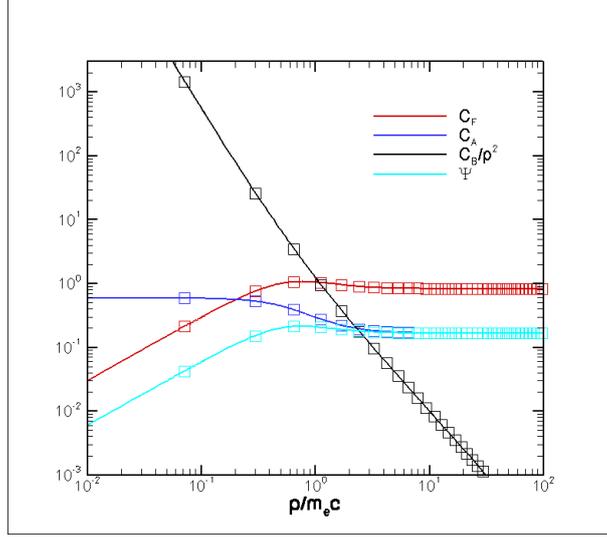
8

Figure 8: Plot of the three collisional coefficients, C_F, C_A, and C_B/p^2, as well as the Chandresekahr function $\Psi(x)$ similar to Fig. 7, but instead for the simulation ran with $\Theta_b = 1/5$, corresponding to $v_t = \sqrt{2/5}c$. Here the squares indicate 20 collocation poiints on the domain $p \in [0, \infty]$, hence no boundary condition is needed for Γ_p at an artificial p_{max}.
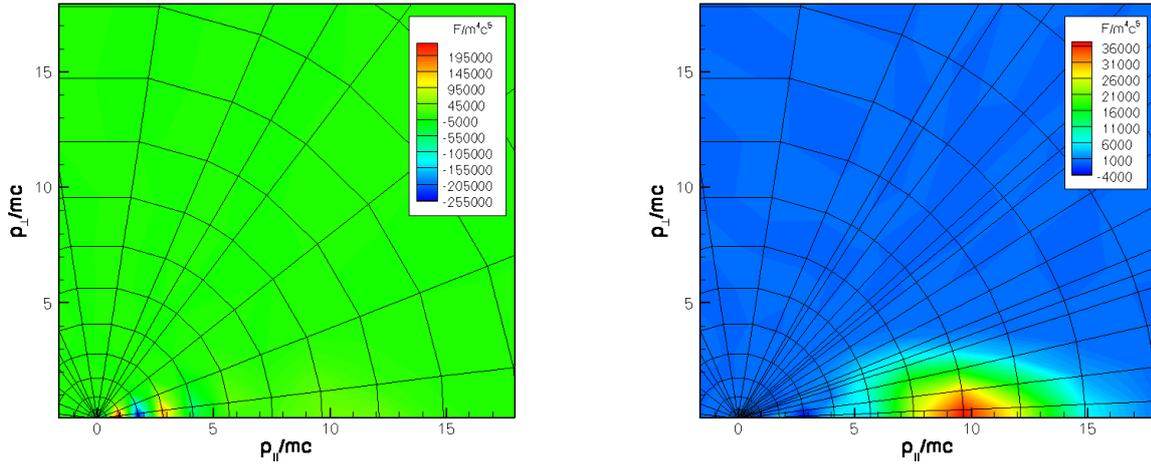

Figure 9: Plots of f_e from a simulation with $\Theta_b = 1/5$ ($v_t = \sqrt{2/5}c$), $\Theta = 1$ evolved to 10 collision times with the full kinetic equation implemented. On the left only 3 cells in ξ were used. On the right, however, two extra cells were included in the right half of the semicircle. This is an advantage of using finite elements with improved accuracy in ξ.
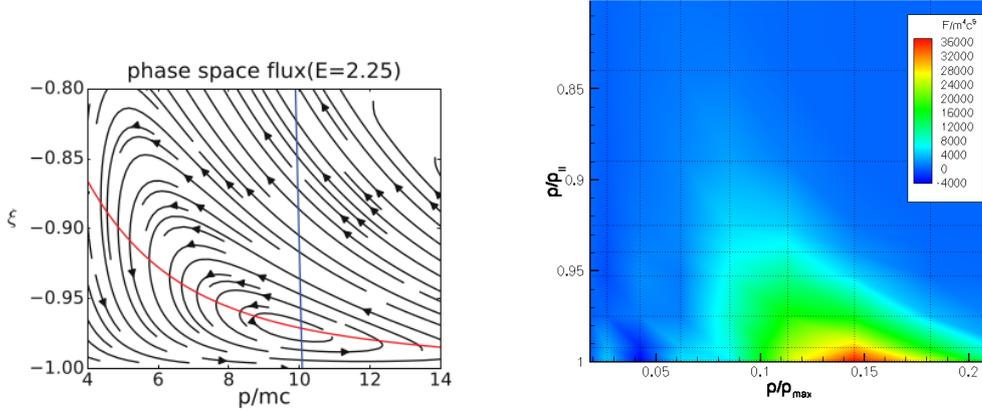
9

Figure 10: The plot on the left is again of the steady-state flow pattern in a 2D relativistic phase space consisting of normalized relativisitc momentum and cosine of pitch angle. The plot on the right shows the distribution function from NIMROD remapped from Fig.9 for comparison with the Guo result. Keep in mind that the plot on the left is the phase space flux whereas the one on the right are the f_e contours.

If you look at our results for running the simulation with the same initial conditions in Guo (shown in Fig. 12), one can see that we were unable to find a steady-state where the distribution would stay put. One could argue that setting the maximum boundary of p at 10 for the simulation may have limited the advancement of the distribution, so we played around with the parameters. For a different run of the simulation we changed $\Theta = 1/5$ and had p be on an infinite domain. Those results are shown in Fig. 9. The major difference between the plots in this figure is how many cells in pitch-angle there are. On the right we included two extra cells, allowing for more detail in the calculation, which let the distribution evolve longer than its counterpart with fewer cells and the simulation ran with the initial conditions in Guo. However, again witht this run no steady-state was found. It is important to note the negative values that pop up in the distribution. This might be a major obstacle that is keeping us from being able to find the steady-state, and we look to address this with future research.

6. Conclusions

Overall, we were unable to find the steady state vortex pattern in phase-space with NIMROD that the Guo paper suggests. However, we were able to add quite a few new features to NIMROD and found some fairly interesting results. One new feature would be the implementation of the free acceleration of a relativistic electron distribution by a constant electric field into NIMROD. We were quite successful with this, checking the accuracy by observing how the distribution held together as well as how well different moments maintained structure through iterations of the code. We were able to put the full kinetic equation into NIMROD and managed to run some simulations, that, although ultimately did not produce the steady-state which we were looking for, were a good stepping stone in the direction of obtaining it. Some steps in the future that we look to add to the code would be a third-order upwinding scheme applied to the advection terms and central order differencing for the diffusive terms to hopefully help deal with the negative numbers that show up around the bulk distribution.
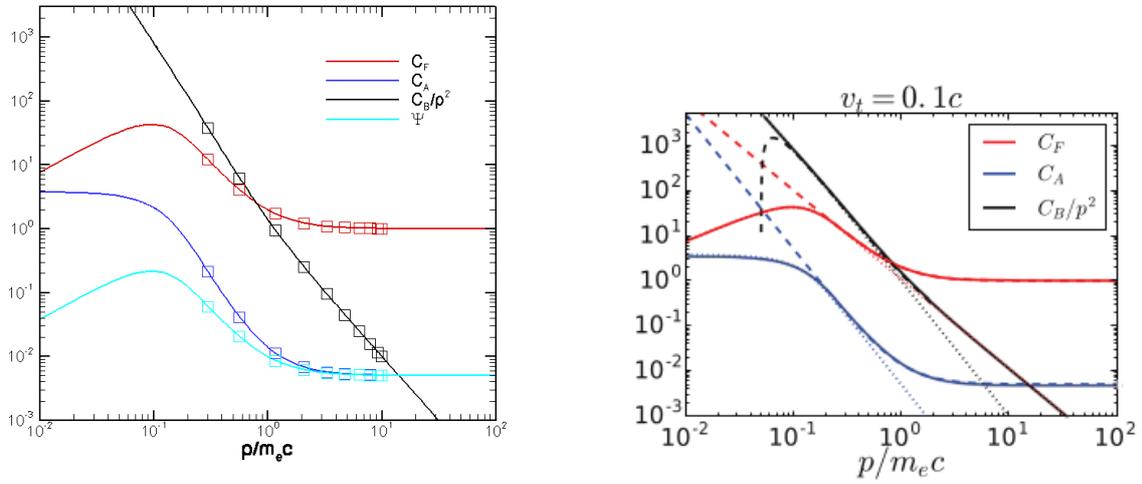
7. Acknowledgements

10

Figure 11: Here again are plots of the collisional coefficients, C_F, C_A, and C_B/p^2 (as well as the Chandresekahr function $\Psi(x)$ on the left) for the parameters of $\Theta_b = 1/200$, meaning the background plasma has $v_T = 0.1c$. On the left we have the results from running the code in NIMROD. On the right we have the results form [3]: the dotted lines correspond to the non-relativistic form, the dashed lines to the relativistic form, and the solid lines are the matched results from their code.

References

[1] A. Stahl, M. Landreman, O. Embréus, T. Fülöp, Norse: A solver for the relativistic non-linear fokker–planck equation for electrons in a homogeneous plasma, Computer Physics Communications 212 (2017) 269–279.

[2] B. N. Breizman, P. Aleynikov, E. M. Hollmann, M. Lehnen, Physics of runaway electrons in tokamaks, Nuclear Fusion 59 (8) (2019) 083001.
doi:10.1088/1741-4326/ab1822.
URL https://doi.org/10.1088/1741-4326/ab1822

[3] Z. Guo, C. J. McDevitt, X.-Z. Tang, Phase-space dynamics of runaway electrons in magnetic fields, Plasma Physics and Controlled Fusion 59 (4) (2017) 044003.
URL http://stacks.iop.org/0741-3335/59/i=4/a=044003

[4] P. Sandquist, S. E. Sharapov, P. Helander, Relativistic electron distribution function of a plasma in a near-critical electric field, Physics of Plasmas 3 (4) (2006) 072108.
URL https://doi.org/10.1063/1.2219428

[5] G. Papp, M. Drevlak, T. Fulop, P. Helander, Runaway electron drift orbits in magnetostatic perturbed fields, Nuclear Fusion 51 (4) (2011) 043004.

[6] E. D. Held, S. E. Kruger, J.-Y. Ji, E. A. Belli, B. C. Lyons, Verification of continuum drift kinetic equation solvers in NIMROD, Physics of Plasmas (Mar. 2015).

[7] C. R. Sovinec, A. H. Glasser, T. A. Gianakon, D. C. Barnes, R. A. Nebel, S. E. Kruger, D. D. Schnack, S. J. Plimpton, A. Tarditi, M. S. Chu, Nonlinear magnetohydrodynamics simulation using high-order finite elements, Journal of Computational Physics 195 (1) (2004) 355–386.
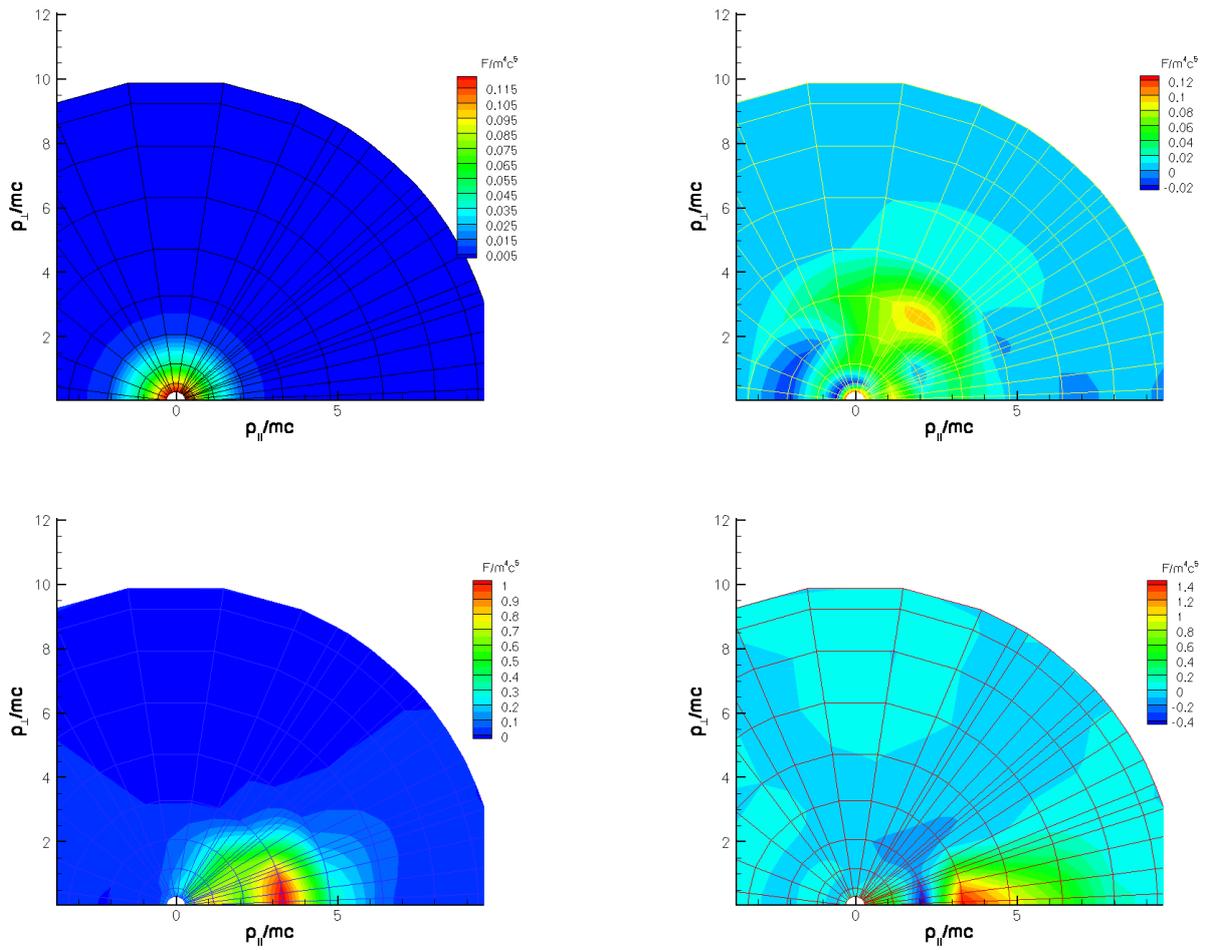
Figure 12: These are four contours depicting the time evolution of the distribution with the full kinetic equation implimented in NIMROD. The initial conditions were $\Theta_b = 1/200$ and with $p_{max} = 10$. Going left to right, we have first the the distribution at t=0, then after 20 collision times, then after 40, and then after 60.